Int. J. Electrochem. Sci., 17 **(2022)** Article Number: 220771, doi: 10.20964/2022.07.72

International Journal of
ELECTROCHEMICAL
SCIENCE
www.electrochemsci.org

Short Communication

Spray-Drying Fabrication and Characterization of $LiTi_{0.05}Mn_{1.95}O_4$@VXC-72R Composite Microspheres as Cathode Materials for Lithium Ion Batteries

Yunhang Liu[1], *Xiangxing Guo*[1], *Xinyang Gao*[1], *Qian Wang*[1], *Lumei Chen*[1], *Yansheng Shen*[1], *Mengyuan Zhao*[1], *Yu Zhou*[1], *Yu Sang*[3], *Qiwen Ran*[2,*], *Hongyuan Zhao*[1,*]

[1] Research Center for Advanced Materials and Electrochemical Technology, School of Mechanical and Electrical Engineering, Henan Institute of Science and Technology, Xinxiang 453003, China
[2] School of Materials and Energy, University of Electronic Science and Technology of China, Chengdu 610054, China
[3] Henan Xinquan Energy Technology Co., Ltd., Xinxiang 453000, China
[*]E-mail: qiwenran@yeah.net, hongyuanzhao@126.com

Received: 6 April 2022 / *Accepted:* 26 May 2022 / *Published:* 6 June 2022

Spherical $LiTi_{0.05}Mn_{1.95}O_4$@VXC-72R was successfully fabricated by spray-drying method with $LiTi_{0.05}Mn_{1.95}O_4$ and VXC-72R nanoparticles as host material and surface modifier. The nanosized $LiTi_{0.05}Mn_{1.95}O_4$ particles were obtained by a simple solid-state reaction process followed with ball-milling treatment. Nano-sized Mn_3O_4 and TiO_2 were applied as manganese precursor and titanium dopant. For the obtained composite microspheres, the introduction of Ti^{4+} ions can reinforce the spinel structure of $LiMn_2O_4$ and avert the decrease of reversible capacity; Nanosized $LiTi_{0.05}Mn_{1.95}O_4$ particles help improve the charge transfer efficiency; VXC-72R inhibits the aggregation of $LiTi_{0.05}Mn_{1.95}O_4$ particles and provide more efficient charge transmission channels; the spherical morphology decreases the surface area of $LiTi_{0.05}Mn_{1.95}O_4$@VXC-72R composite, which can enhance the surface stability of active material. Thanks to the synergistic interaction of these positive functions, the $LiTi_{0.05}Mn_{1.95}O_4$@VXC-72R sample presented superior cycling performance at 1.0 C (100 cycles, Retention: 93.9%; initial discharge capacity: 120.8 mAh g^{-1}) Furthermore, both high-rate performance and high-temperature cycling stability were improved to a certain extent.

Keywords: Cathode material; $LiMn_2O_4$; Ti-doping; VXC-72R nanoparticles; Spherical morphology; Electrochemistry performance

1. INTRODUCTION

With the development of new energy industry, lithium-ion batteries are important to deal with the energy crisis and environmental pollution. As one kind of commercialized cathode materials, lithium manganate oxides ($LiMn_2O_4$) were applied in the field of power supply and energy storage because of

the high performance-price ratio and good safety performance [1-3]. It should be noted that the electrochemical property has severely disrupted the application of $LiMn_2O_4$ in the field of high-end power lithium-ion batteries [4-6].

The cycling property of $LiMn_2O_4$ is intimately connected to the practical application of cathode materials [7-10]. To enhance the cycling property of $LiMn_2O_4$, many modification approaches such as body-doping, surface coating, and morphology controlling were proposed to optimize the structural stability and surface morphology [11-16]. Among the aforementioned modification strategies, the doping approach can effectively reinforce the spinel structure of $LiMn_2O_4$ by replacing manganese ions with other heterogeneous ions (F^-, Li^+, Zn^{2+}, Mg^{2+}, Al^{3+}, Ti^{4+}) [14, 17-21]. Especially, the high valence Ti^{4+} ions not only improve the structural stability of $LiMn_2O_4$ but also avert the decrease of Mn^{4+} ions in the crystal structure of $LiMn_2O_4$, which has much to do with the reversible capacity [21, 22]. Xiong et al. prepared the titanium-doped $LiMn_2O_4$ samples through a simple solid-state sintering process [21]. Electrochemical measurement showed that the $LiMn_{1.97}Ti_{0.03}O_4$ sample possessed good cycling performance with high reversible capacity, which is closely associated with the positive function of Ti^{4+} ions. Several other reported works also confirmed the impact of titanium-doping on the cycling stability of $LiMn_2O_4$ [23, 24]. Furthermore, Zhao et al. reported the preparation of $LiMn_2O_4$ and carbon black nanoparticles composite through the spray-drying process [25]. The combination of carbon black nanoparticles and spherical morphology can contribute to the enhancement of cycling property and rate performance due to the decreased manganese dissolution, charge transfer efficiency, and uniform distribution of carbon black nanoparticles with high electronic conductivity.

In this work, we fabricated the spherical $LiTi_{0.05}Mn_{1.95}O_4$@VXC-72R composite with $LiTi_{0.05}Mn_{1.95}O_4$ and VXC-72R nanoparticles as host material and surface modifier. The nanosized $LiTi_{0.05}Mn_{1.95}O_4$ particles were obtained by a simple solid-state reaction process followed with ball-milling treatment. Nano-sized Mn_3O_4 and TiO_2 were applied as manganese precursor and titanium dopant. The cycling performance, rate capacity, and elevated temperatures properties were investigated in detail.

2. EXPERIMENTAL

To prepare the $LiTi_{0.05}Mn_{1.95}O_4$@VXC-72R composite microspheres, the $LiTi_{0.05}Mn_{1.95}O_4$ octahedrons were obtained by a simple solid-state reaction process followed with ball-milling treatment. Nano-sized Mn_3O_4 and TiO_2 were applied as manganese precursor and titanium dopant. According to the chemical formula, $LiOH{\cdot}H_2O$ (Excessive amount: 5%), octahedral Mn_3O_4 and nanosized TiO_2 were mixed evenly and calcinated in high temperature muffle furnace (780 °C, 10 h) followed with the ball-milling treatment to obtain the nanosized $LiTi_{0.05}Mn_{1.95}O_4$. And then, VXC-72R nanoparticles (0.72 g) and $LiTi_{0.05}Mn_{1.95}O_4$ nanoparticles (11.28 g) were evenly dispersed into the deionized water. The black mixed slurry was spray-dried for the preparation of the spherical $LiTi_{0.05}Mn_{1.95}O_4$@VXC-72R composite (Drying temperature: 180 °C).

The influence of Ti-doping and VXC-72R on the phase structure and surface morphologies of the spherical $LiTi_{0.05}Mn_{1.95}O_4$@VXC-72R composite was characterized by XRD and SEM analysis

techniques. XRD pattern was applied to study the on the phase structure, and SEM image was used to confirm the surface morphology. The electrochemical performance of the spherical $LiTi_{0.05}Mn_{1.95}O_4$@VXC-72R composite were obtained by LANHE CT2001A battery tester.

3. RESULT AND DISCUSSION

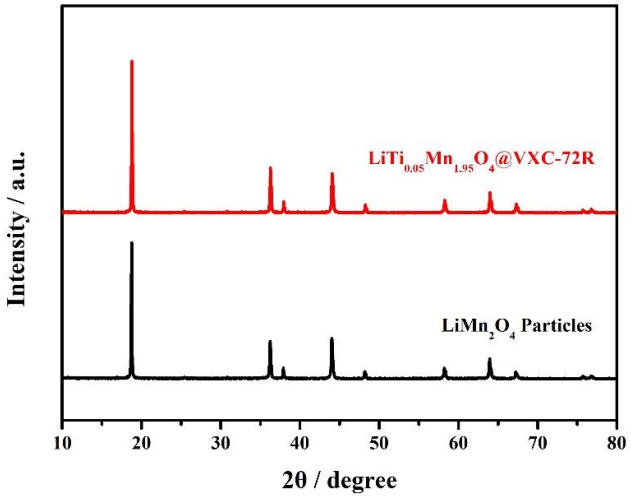

Figure 1. XRD patterns of spherical $LiTi_{0.05}Mn_{1.95}O_4$@VXC-72R composite and $LiMn_2O_4$ particles.

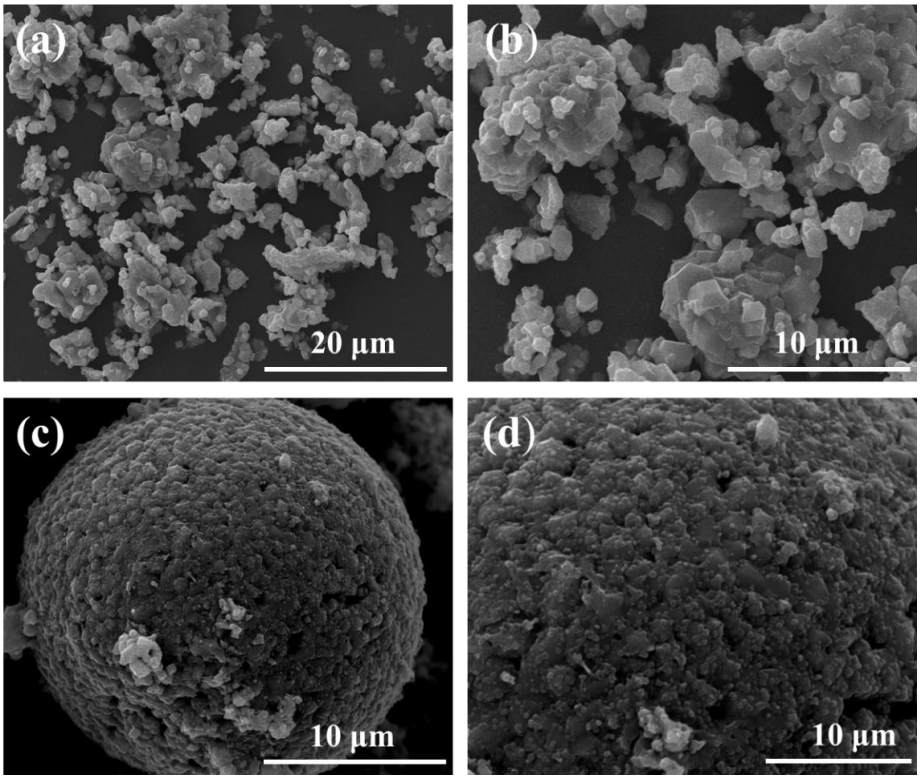

Figure 2. SEM images of (a, b) $LiMn_2O_4$ particles and (c, d) spherical $LiTi_{0.05}Mn_{1.95}O_4$@VXC-72R composite.

Figure 1 provides the XRD analysis results of the spherical $LiTi_{0.05}Mn_{1.95}O_4$@VXC-72R composite and $LiMn_2O_4$ particles. It can be observed that these two spinel samples present apparent diffraction peaks of $LiMn_2O_4$ [9, 24, 25]. Moreover, other peaks of MnO_2 particles, Mn_3O_4 octahedrons and TiO_2 nanoparticles was not seen in the aforementioned XRD analysis results, which means the complete transformation of MnO_2 or Mn_3O_4 to $LiMn_2O_4$ samples [21, 24]. Figure 2 provides the SEM analysis results of the spherical $LiTi_{0.05}Mn_{1.95}O_4$@VXC-72R composite and $LiMn_2O_4$ particles. It can be found from Figure 2(a, b) that $LiMn_2O_4$ particles prepared from MnO_2 particles present inhomogeneous particle size distribution.

Figure 2(c, d) provides the SEM analysis results of $LiTi_{0.05}Mn_{1.95}O_4$@VXC-72R composite microspheres prepared from Mn_3O_4 octahedrons and TiO_2 nanoparticles. It can be found that the obtained composite microspheres fabricated by spray-drying method presents apparent spherical morphology, which helps decrease the surface area. The dissolution of surface manganese can be inhibited to a certain degree because of the decreased contact area of composite microspheres with electrolyte [25]. The uniform distribution of VXC-72R nanoparticles with high electronic conductivity can not only inhibit the aggregation of $LiTi_{0.05}Mn_{1.95}O_4$ particles but also provide more efficient charge transmission channels [26].

The initial charge-discharge curve can provide some important information about the electrochemical reaction. Figure 3 provides the corresponding charge-discharge curves of spherical $LiTi_{0.05}Mn_{1.95}O_4$@VXC-72R composite and $LiMn_2O_4$ particles. It can be found that both the undoped $LiMn_2O_4$ and $LiTi_{0.05}Mn_{1.95}O_4$@VXC-72R composite microspheres possess similar initial charge-discharge curves. The apparent voltage platforms around 4.10 and 3.95 V in the initial discharge curves agree with the corresponding characteristic voltage platforms of $LiMn_2O_4$, which indicates that both the Ti^{4+} ions doping and spherical morphology does not have the influence on the lithium intercalation process [24, 25].

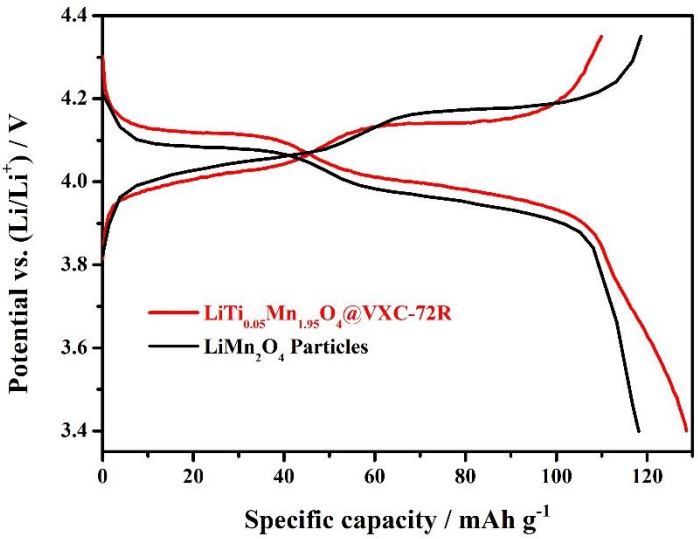

Figure 3. Initial charge-discharge curves of spherical $LiTi_{0.05}Mn_{1.95}O_4$@VXC-72R composite and $LiMn_2O_4$ particles.

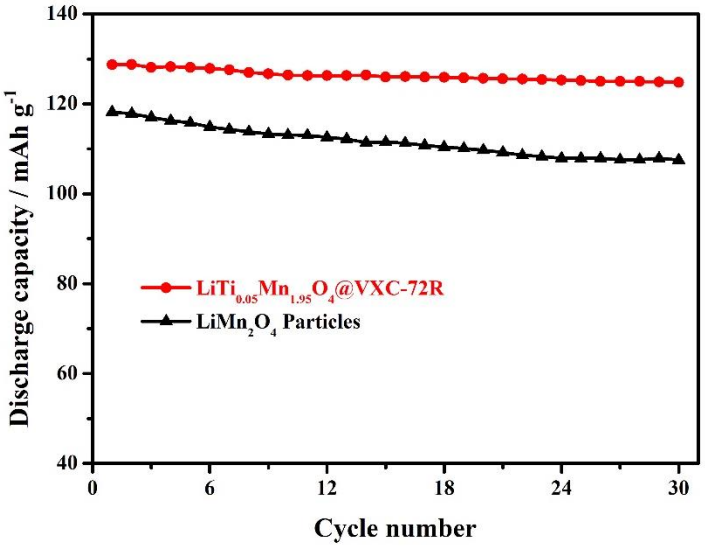

Figure 4. Cycling stability of spherical $LiTi_{0.05}Mn_{1.95}O_4$@VXC-72R composite and $LiMn_2O_4$ particles cycled at 0.5 C.

Figure 4 provides the cycling property of the spherical $LiTi_{0.05}Mn_{1.95}O_4$@VXC-72R composite and $LiMn_2O_4$ particles cycled at 0.5 C. As shown here, the undoped $LiMn_2O_4$ presents low initial discharge capacity of 118.2 mAh g^{-1} with poor cycling performance. After 30 cycles, the discharge capacity decreases to 107.5 mAh g^{-1} with low retention rate of 90.9%. For the obtained spherical $LiTi_{0.05}Mn_{1.95}O_4$@VXC-72R composite, the better cycling property can be achieved with higher capacity retention rate of 97.0% (Initial discharge capacity: 128.7 mAh g^{-1}), which can be further observed form the histogram of initial capacity and retention shown in Figure 5. Such good electrochemical property has much to do with the synergistic interaction of Ti-doping, VXC-72R nanoparticles, and spherical morphology [23, 25].

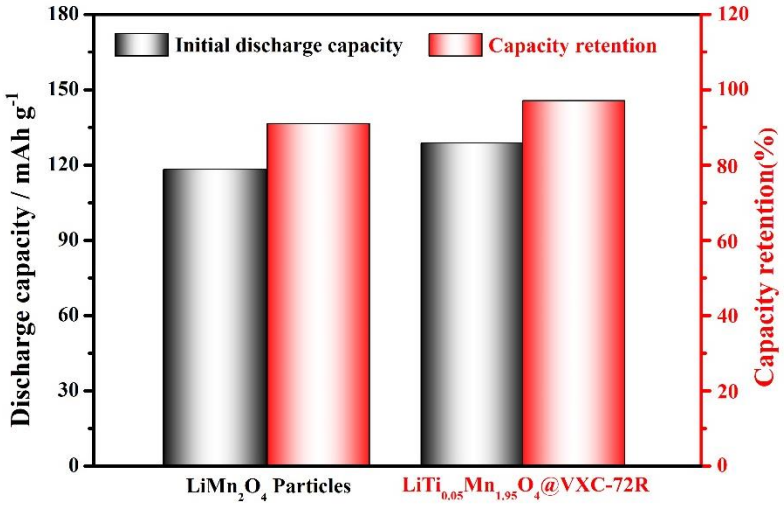

Figure 5. Histogram of initial discharge capacity and capacity retention of spherical $LiTi_{0.05}Mn_{1.95}O_4$@VXC-72R composite and $LiMn_2O_4$ particles cycled at 0.5 C.

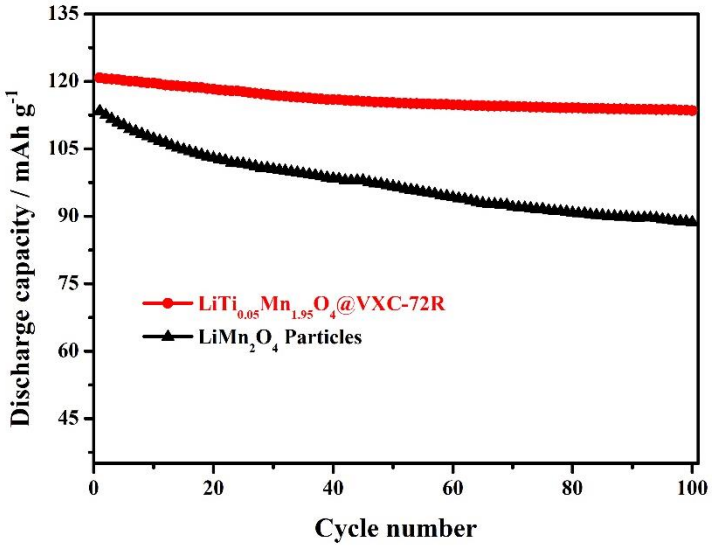

Figure 6. Long cycling performance of spherical $LiTi_{0.05}Mn_{1.95}O_4$@VXC-72R composite and $LiMn_2O_4$ particles cycled at 1.0 C.

Long cycling stability is of great significance to the practical application of spherical $LiTi_{0.05}Mn_{1.95}O_4$@VXC-72R composite. Figure 6 provides the corresponding long cycling stability of these two samples cycled at 1.0 C. It can be found that the $LiMn_2O_4$ sample exhibit poor cycling performance with low discharge capacity, which has much to do with the agglomerated particles [8, 27]. The 100th discharge capacity decreases to 88.7 mAh g^{-1} after 100 cycles (Retention rate: 78.2%). For the obtained spherical $LiTi_{0.05}Mn_{1.95}O_4$@VXC-72R composite, the better cycling property can be achieved after 100 cycles with higher retention rate of 93.9% (Initial capacity: 120.8 mAh g^{-1}). Such superior cycling property is intimately connected to the synergistic interaction of Ti-doping, VXC-72R nanoparticles, and spherical morphology: (1) The Ti^{4+}-doping can strengthen the structure stability of $LiMn_2O_4$ and replace a certain amount of Mn^{4+} ions, which contributes to the high reversible capacity [23, 24]; (2) The nanosized $LiTi_{0.05}Mn_{1.95}O_4$ particles help improve the transmission efficiency of lithium ions due to the nanosized particle size [9, 28]; (3) The well-distributed VXC-72R nanoparticles with high electrical conductivity inhibit the aggregation of $LiTi_{0.05}Mn_{1.95}O_4$ particles and provide more efficient charge transmission channels [7, 10]; (4) The spherical morphology decreases the surface area of $LiTi_{0.05}Mn_{1.95}O_4$@VXC-72R composite, which can decrease the manganese dissolution to a certain degree because of the decreased contact area of composite microspheres with electrolyte [25, 26]. Table 1 lists the comparison of long cycling performance of $LiTi_{0.05}Mn_{1.95}O_4$@VXC-72R composite microspheres and other cathode materials for lithium-ion batteries. It can be found that the $LiTi_{0.05}Mn_{1.95}O_4$@VXC-72R composite microspheres present better cycling performance compared to other $LiMn_2O_4$-based cathode materials for lithium-ion batteries, which is intimately connected to the the synergistic interaction of Ti-doping, VXC-72R nanoparticles, and spherical morphology.

Table 1. Long cycling performance of $LiTi_{0.05}Mn_{1.95}O_4$@VXC-72R composite microspheres and other cathode materials for lithium-ion batteries [21-23].

Sample	Cycling condition	Initial capacity (mAh g^{-1})	Capacity retention (%)	Reference
$LiMn_2O_4$ nanoparticles	1.0 C, 100 cycles	114.0	87.8	[22]
$LiMn_{1.97}Ti_{0.03}O_4$ particles	0.5 C, 70 cycles	135.7	95.0%	[21]
$LiMn_{1.97}Ti_{0.03}O_4$ nanorods	0.5 C, 100 cycles	125.1	93.8	[23]
$LiTi_{0.05}Mn_{1.95}O_4$@VXC-72R composite microspheres	1.0 C, 100 cycles	120.8	93.9%	This work

Figure 7 provides the rate property of spherical $LiTi_{0.05}Mn_{1.95}O_4$@VXC-72R composite and $LiMn_2O_4$ particles. The cycling charge-discharge rate produces obvious impact on the discharge capacity. These two samples show more obvious changes with the increasing of cycling rate. When tested at 10 C, the discharge capacity of $LiMn_2O_4$ sample shows a large capacity attenuation. The discharge capacity rapidly decrease to 43.4 mAh g^{-1} with low retention rate of 38.4% compared to the 1st discharge capacity. For the obtained spherical $LiTi_{0.05}Mn_{1.95}O_4$@VXC-72R composite, the cycling property is much better than that of the $LiMn_2O_4$ particles. The discharge capacity can reach up to 87.1 mAh g^{-1} at 10 C. Such superior rate capability is intimately connected to the synergistic interaction of Ti-doping, VXC-72R nanoparticles, and spherical morphology [23, 25, 26].

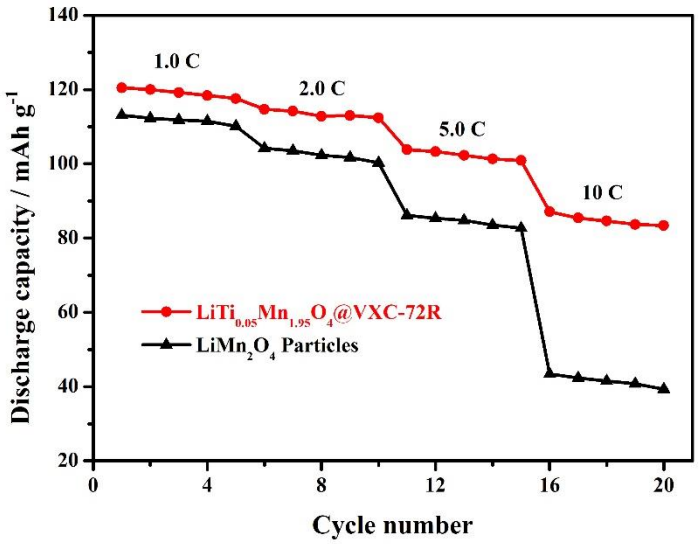

Figure 7. Rate capability of spherical $LiTi_{0.05}Mn_{1.95}O_4$@VXC-72R composite and $LiMn_2O_4$ particles.

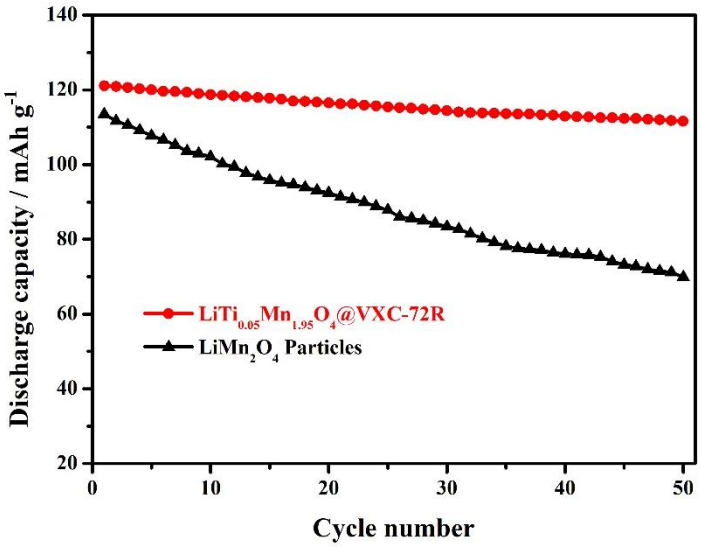

Figure 8. Elevated-temperature cycling property of spherical $LiTi_{0.05}Mn_{1.95}O_4$@VXC-72R composite and $LiMn_2O_4$ particles.

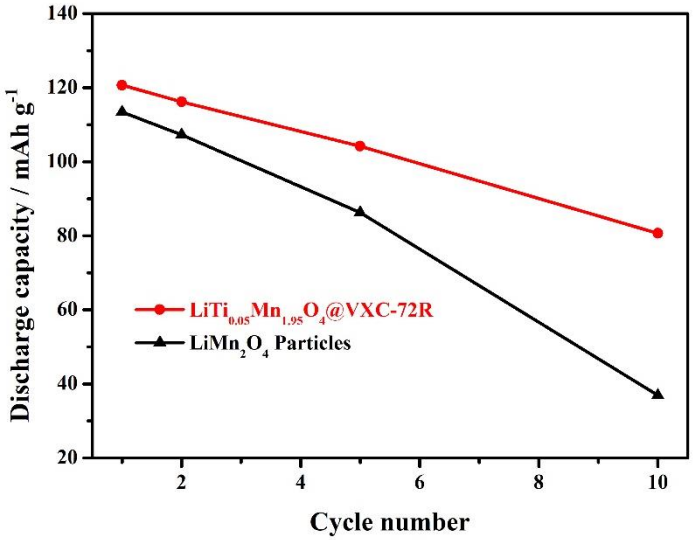

Figure 9. Elevated-temperature rate capability of spherical $LiTi_{0.05}Mn_{1.95}O_4$@VXC-72R composite and $LiMn_2O_4$ particles.

Figure 8 provides the cycling property of spherical $LiTi_{0.05}Mn_{1.95}O_4$@VXC-72R composite and $LiMn_2O_4$ particles cycled at 1.0 C under high temperature (55 °C). The unmodified $LiMn_2O_4$ sample exhibit poor cycling performance with low discharge capacity, which has much to do with the agglomerated particles. The 50th discharge capacity decreases to 69.9 mAh g^{-1} after 50 cycles (Retention rate: 61.6%). For the obtained spherical $LiTi_{0.05}Mn_{1.95}O_4$@VXC-72R composite, the better cycling property can be achieved after 50 cycles with higher retention rate of 92.2% (50th capacity: 111.6 mAh g^{-1}). Figure 9 provides the corresponding rate property of these two samples under high temperature (55 °C). When tested at 10 C, the discharge capacity of $LiMn_2O_4$ sample shows a large capacity

attenuation. The discharge capacity rapidly decrease to 36.9 mAh g^{-1}. For the obtained spherical $LiTi_{0.05}Mn_{1.95}O_4$@VXC-72R composite, the cycling property is much better than that of the $LiMn_2O_4$ particles. The discharge capacity can reach up to 80.7 mAh g^{-1} at 10 C. Such superior cycling property is intimately connected to the synergistic interaction of Ti-doping, VXC-72R nanoparticles, and spherical morphology

4. CONCLUSIONS

A spray-drying strategy was successfully applied to fabricate the $LiTi_{0.05}Mn_{1.95}O_4$@VXC-72R composite microspheres with $LiTi_{0.05}Mn_{1.95}O_4$ and VXC-72R nanoparticles as host material and surface modifier. The nanosized $LiTi_{0.05}Mn_{1.95}O_4$ particles were obtained by a simple solid-state reaction followed with ball-milling treatment. For the composite microspheres, the synergistic combination of Ti-doping, VXC-72R nanoparticles, and spherical morphology enhanced the cycling performance, rate property, and elevated-temperature cycling property.

ACKNOWLEDGMENTS
This work was financially supported by the Natural Science Foundation of Henan Province (No. 202300410163) and University Students' Innovation and Pioneering Project of Henan Province (No. S202110467037X).

References

1. Q. Liu, Q. Liang, J. Guo, M. Xiang, W. Bai, H. Bai and X. Liu, *Ceramics International*, 47 (2021) 2441.
2. H. Liu, M. Li, M. Xiang, J. Guo, H. Bai, W. Bai and X. Liu, *Journal of Colloid and Interface Science*, 585 (2021) 729.
3. J. Zhao, M. Shi, Y. Wu, P. Zhang, X. Tan, X. Kang, W. Chu, Z. Wu and Y. Li, *Colloids and Surfaces A: Physicochemical and Engineering Aspects*, 634 (2022) 127932.
4. Y. Li, J. Zhi, B. Xue and P. Chen, *Materials Chemistry and Physics*, 276 (2022) 125331.
5. Y.H. Ikuhara, X. Gao, K. Kawahara, C.A.J. Fisher, A. Kuwabara, R. Ishikawa, H. Moriwake and Y. Ikuhara, *ACS Applied Materials & Interfaces*, 14 (2022) 6507.
6. W. Xu, Y. Zheng, Y. Cheng, R. Qi, H. Peng, H. Lin and R. Huang, *ACS Applied Materials & Interfaces*, 13 (2021) 45446.
7. J. Cao, S. Guo, R. Yan, C. Zhang, J. Guo and P. Zheng, *Journal of Alloys and Compounds*, 741 (2018) 1.
8. X. Liang, S. Zeng, Y. Liu, L. Shi and T. Liu, *Materials Science and Technology*, 31 (2014) 443.
9. H. Xia, Z. Luo and J. Xie, *Progress in Natural Science: Materials International*, 22 (2012) 572.
10. S. Lee, Y. Cho, H.K. Song, K.T. Lee and J. Cho, *Angewandte Chemie International Edition*, 51 (2012) 8748.
11. J. Guo, Y. Chen, C. Xu, Y. Li, S. Deng, H. Xu and Q. Su, *Ionics*, 25 (2019) 2977.
12. H. Zhao, F. Li, X. Bai, T. Wu, Z. Wang, Y. Li and J. Su, *Materials (Basel)*, 11 (2018) 1302.
13. H. Zhao, D. Li, Y. Wang, F. Li, G. Wang, T. Wu, Z. Wang, Y. Li and J. Su, *Materials (Basel)*, 11 (2018) 1455.
14. J. Liu, G. Li, H. Bai, M. Shao, C. Su, J. Guo, X. Liu and W. Bai, *Solid State Ionics*, 307 (2017) 79.
15. L.-X. Zhang, Y.-Z. Wang, H.-F. Jiu, Y.-L. Wang, Y.-X. Sun and Z. Li, *Electronic Materials Letters*,

10 (2014) 439.
16. Q. Liu, S. Wang, H. Tan, Z. Yang and J. Zeng, *Energies*, 6 (2013) 1718.
17. W. Wen, B. Ju, X. Wang, C. Wu, H. Shu and X. Yang, *Electrochimica Acta*, 147 (2014) 271.
18. D. Arumugam, G.P. Kalaignan, K. Vediappan and C.W. Lee, *Electrochimica Acta*, 55 (2010) 8439.
19. H. Zhao, F. Li, X. Liu, C. Cheng, Z. Zhang, Y. Wu, W. Xiong and B. Chen, *Electrochimica Acta*, 151 (2015) 263.
20. J.L. Wang, Z.H. Li, J. Yang, J.J. Tang, J.J. Yu, W.B. Nie, G.T. Lei and Q.Z. Xiao, *Electrochimica Acta*, 75 (2012) 115.
21. L. Xiong, Y. Xu, C. Zhang, Z. Zhang and J. Li, *Journal of Solid State Electrochemistry*, 15 (2010) 1263.
22. L. Xiong, Y. Xu, T. Tao and J.B. Goodenough, *Journal of Power Sources*, 199 (2012) 214.
23. Xue Jing, Zhang Hu, Yang Tuoying and Z. Xiuxing, *International Journal of Electrochemical Science*, (2020) 8732.
24. Y. Li, G. Zhu, Q. Ran, J. Liu, Y. Zhou, M. Zhao, P. Cao and H. Zhao, *International Journal of Electrochemical Science*, (2021).
25. H. Zhao, Y. Li, D. Shen, Q. Yin and Q. Ran, *Journal of Materials Research and Technology*, 9 (2020) 7027.
26. H. Zhao, N. Hu, R. Xu, H. Liu, J. Liu and Q. Ran, *Ceramics International*, 46 (2020) 21805.
27. Z. Cai, Y. Ma, X. Huang, X. Yan, Z. Yu, S. Zhang, G. Song, Y. Xu, C. Wen and W. Yang, *Journal of Energy Storage*, 27 (2020).
28. P. Ragupathy, H.N. Vasan and N. Munichandraiah, *Materials Chemistry and Physics*, 124 (2010) 870